frontiers | Frontiers in Earth Science

ORIGINAL RESEARCH
published: 08 July 2022
doi: 10.3389/feart.2022.932263

Can Eu Anomaly Indicate a Hydrothermal Fluid Si Source? A Case Study of Chert Nodules From the Permian Maokou and Wujiaping Formations, South China

Chenqing Li[1,2], *Yixin Cui*[3]*, *Meng Ning*[4], *Chao Li*[5], *Chaochao Xing*[1,2], *Pan Xia*[4] and *Lin Dong*[1,2]*

[1]Key Laboratory of Orogenic Belts and Crustal Evolution, MOE, Beijing, China, [2]School of Earth and Space Science, Peking University, Beijing, China, [3]Petroleum Exploration and Production Research Institute, SINOPEC, Beijing, China, [4]State Key Laboratory of Oil and Gas Reservoir Geology and Exploitation and Institute of Sedimentary Geology, Chengdu University of Technology, Chengdu, China, [5]Institute of Mineral Resources, Chinese Academy of Geological Sciences, Beijing, China

OPEN ACCESS

Edited by:
Shu Jiang,
The University of Utah, United States

Reviewed by:
Zheyu Tian,
University College London, United Kingdom
Qing Ouyang,
Nanjing Institute of Geology and Palaeontology (CAS), China

***Correspondence:**
Yixin Cui
cuiyixin.syky@sinopec.com
Lin Dong
lin.dong@pku.edu.cn

Specialty section:
This article was submitted to Structural Geology and Tectonics, a section of the journal Frontiers in Earth Science

Received: 29 April 2022
Accepted: 03 June 2022
Published: 08 July 2022

Citation:
Li C, Cui Y, Ning M, Li C, Xing C, Xia P and Dong L (2022) Can Eu Anomaly Indicate a Hydrothermal Fluid Si Source? A Case Study of Chert Nodules From the Permian Maokou and Wujiaping Formations, South China. Front. Earth Sci. 10:932263. doi: 10.3389/feart.2022.932263

The Middle–Late Permian witnessed an unusual chert accumulation event along the margin of the Pangea and Paleo-Tethys realms, known as the "Permian Chert Event (PCE)." The PCE is well recognized in the Permian limestone from South China, in the forms of nodular and bedded cherts. Previous studies suggested that PCE was caused by hydrothermal fluids related to the Emeishan large igneous province (ELIP). Meanwhile, another hypothesis supported the biogenic origin of PCE, i.e., the Permian chert derived from biosilicification of abundant sponges and radiolarian. Thus, sources of silica from the Permian chert remain uncertain. To understand linkages among PCE, biosilicification mechanism, and the ELIP event, this study focused on chert nodules collected from the Permian Maokou and Wujiaping formations in the Lianziya and Maoertang sections, South China. We measured germanium/silicon ratios (Ge/Si) and rare earth element (REE) compositions of chert nodules on the basis of petrographic analysis. Ge/Si ratios range from 0.14 to 0.63 μmol/mol with an average of 0.33 μmol/mol (n=18) in the Lianziya section and from 0.02 to 0.75 μmol/mol with an average of 0.18 μmol/mol (n=45) in the Maoertang section, both of which are close to the seawater value. The REE pattern is characterized by LREE depleted with a positive Eu anomaly ranging from 0.66 to 2.16 in the Lianziya section and from 1.05 to 9.57 in the Maoertang section. Our results indicate that the silica of the Permian chert predominantly originated from seawater with limited contributions from hydrothermal fluids. To further quantify the contributions of hydrothermal fluids, we applied a binary (seawater and hydrothermal fluid) mixing model based on two geochemical proxies, i.e., the Ge/Si ratio and Eu anomaly. The modeling results suggest a mixing of 0.5 vol% to 1 vol% hydrothermal fluids with contemporaneous seawater, verifying the dominant seawater source of silica in the PCE. Although it has been widely accepted that positive Eu anomaly points to the hydrothermal fluid origin of silica, our study demonstrates that positive Eu anomaly could also be present in cherts that was

predominantly derived from normal seawater. Therefore, the analysis of the Ge/Si ratio or REE compositions is highly recommended when determining the Si source of cherts.

Keywords: germanium to silicon ratio (Ge/Si), chert nodules, hydrothermal fluids, Eu anomaly, Permian, rare earth element (REE)

1 INTRODUCTION

Chert nodules and bedded chert are of great geological significance for their strong weathering resistance and various silica sources (Maliva et al., 1989; Sugitani, 1992; Racki, 1999; Beauchamp and Baud, 2002; Kato and Nakamura, 2003). A remarkable chert accumulation event, the "Permian Chert Event (PCE)", occurred in the Middle-Late Permian (Beauchamp and Baud, 2002; Yao et al., 2013; Gao et al., 2020; Yu et al., 2020; Zheng et al., 2021). The Permian cherts were distributed in the margin of the Pangea and the Paleo-Tethys realm (Beauchamp and Baud, 2002; Yao et al., 2013; Dong et al., 2020; Yao et al., 2021). One hypothesis attributes chert formation around the Pangea to the upwelling of cold bottom seawater. Large amounts of nutrients were carried by the bottom seawater, facilitating the blooming of siliceous organisms (Beauchamp and Baud, 2002; Gates et al., 2004). The cold bottom seawater could be derived from glacier melting or wind-driven fluxes along the margin of the Pangea (Yu et al., 2020). It was also suggested that the PCE in the South China Block (SCB) might be triggered by various factors: 1) biologic origin, which became one of the most vital Si sources for cherts in the SCB, with the dramatic evolution of siliceous organisms (Beauchamp and Baud, 2002; Yao et al., 2013; Gao et al., 2020; Yu et al., 2020; Zheng et al., 2021); 2) tectonic activities, which could create extra space for crystal growth, elevate temperature, and induce silica-rich hydrothermal fluids that were saturated with respect to silica when moving up and precipitate as cherts (Dong et al., 2020; Yao et al., 2021); 3) the Emeishan Large Igneous Province (ELIP), which, evidenced by intense tectonic events and hydrothermal activities, is dated to 260 ± 3 Ma (Shellnutt, 2014) and might have led to formation of the PCE cherts (Dong et al., 2020; Zheng et al., 2021). However, there is no consensus on the Si sources of the PCE cherts.

The reservoirs of silicon mainly include normal seawater, hydrothermal fluids, and biological silica sinks (Maliva et al., 1989; Maliva et al., 2005). A series of geochemical proxies, such as germanium/silicon ratio (Ge/Si), Eu anomaly (Eu/Eu*), Al/(Al + Fe + Mn), Fe_2O_3/TiO_2, and $Al_2O_3/(Al_2O_3 + Fe_2O_3)$ diagram, Co/Ni, Co × Mn, and Cd/Mo diagram have been widely used in determining Si sources (Murray et al., 1991; Murray, 1994; Shen et al., 2011; Dong et al., 2015; Shen et al., 2018; Cui et al., 2019). In this study, two geochemical proxies, Ge/Si ratio and Eu anomaly, are used to constrain the Si source of the Maokou and Wujiaping cherts in the SCB.

According to the apparent variations of Ge/Si ratios in different reservoirs, Ge/Si ratios are widely applied in tracing the Si source of chert formations (Tribovillard, 2013; Alibert and Kinsley, 2016; Tatzel et al., 2017; Cui et al., 2019; Guan et al., 2020; Deng et al., 2022). Germanium (Ge) and silicon (Si) belong to the same group (IVA) in the periodic table of elements and possess similar chemical characteristics (Bernstein, 1985). However, because of its larger atomic radius, Ge performs differently in low- and high-temperature geological processes compared to Si (Bernstein, 1985; Bernstein and Waychunas, 1987), leading to significant variations of Ge/Si (μmol/mol) ratios in various reservoirs (Bernstein, 1985; Baronas et al., 2017). Ge/Si ratio of hydrothermal fluids is about 9 μmol/mol, which is one order of magnitude higher than that of seawater (Ge/Si_{sw} = 0.72 μmol/mol) and river water (Ge/Si_{rw} = 0.58 μmol/mol) (Froelich et al., 1992; Mortlock et al., 1993; Escoube et al., 2015). Because biogenic silica does not fractionate Ge from Si, the Ge/Si ratios of siliceous organisms are close to those of seawater/river water. For instance, Ge/Si ratios of diatoms, siliceous sponges, and radiolarians range between 0.45 and 0.78 μmol/mol, 0.08–0.38 μmol/mol and 0.62–1.57 μmol/mol, respectively (Shemesh et al., 1989; Bareille et al., 1998; Tribovillard et al., 2011; Tribovillard, 2013).

The rare earth elements (REE) of cherts are difficult to fractionate during diagenetic process and have unique chemical characteristics in different reservoirs (Elderfield et al., 1988; Bau, 1991; Sholkovitz, 1992; Sholkovitz et al., 1994). Therefore, REE patterns and related proxies can be used to trace Si sources. For example, seawater-sourced chert shows a light REE-depleted pattern, with a negative Ce anomaly and a high Y/Ho. In contrast, chert originating from hydrothermal fluids has a flat REE pattern with a high Eu anomaly. High-temperature fluids preferentially take in Eu^{2+} from oceanic crust by water-rock reaction under acidic conditions (Elderfield et al., 1988), leading to an enrichment of Eu in hydrothermal fluids (Bau, 1991; Douville et al., 1999). Positive Eu anomaly of hydrothermal fluids [with an average of 14.17 (Mills and Elderfield, 1995)] is higher than that of seawater and river [1.13 and 0.76, respectively (Alibo and Nozaki, 1999; Soyol-Erdene and Huh, 2013)].

To constrain the Si source of the PCE chert nodules in the SCB, we collected chert nodules from two sections and conducted petrographic and geochemical analyses.

2 GEOLOGICAL SETTING

The South China Block (SCB) is composed of the Yangtze Platform to the northwest and the Cathaysia Old Land to the southeast, separated by the Jiangnan Orogen (Wang and Jin, 2000; Shen et al., 2019). In the SCB, the Permian successions, consisting of the Liangshan member, Qixia, Maokou, Longtan/Wujiaping, and Changxing formations in ascending order, vary from 120 to 1,200 m thick, and are well constrained by biostratigraphic framework. The Yunan movement in the Late

Carboniferous caused a big unconformity, the Permian successions began with the Liangshan Member (Shen et al., 2019; Shen et al., 2021). The Maokou Formation, with a thickness of 120–300 m, conformably overlies the Qixia Formation. It is composed of light gray limestone with bedded cherts and nodular cherts (Liu et al., 2020). There is a widespread parallel unconformity between the Maokou and Wujiaping formations, which is caused by the Dongwu movement (Shen et al., 2019). The Wujiaping Formation consists of 60–90 m-thick gray limestone intercalated with bedded/nodular cherts and coals. Emeishan large igneous province (ELIP) event occurred around 260 Ma (Shellnutt, 2014), leading to intense basalt weathering. The overlying upper Permian Changxing Formation is mainly composed of thick limestone intercalated with minor dolomitic limestone.

This study focuses on the Maoertang and Lianziya sections. The Maoertang section (105°25′3″N, 32°16′23″E) is located in Jiange County, Guangyuan City, Sichuan Province, which is in the transition zone between Songpan-Ganzi fold belt and southern part of Hannan-Micang Mountain uplift (Regional Geology of Sichuan Province, 1991). The Lianziya Section (110°47′20″N, 30°56′21″E) located in Zigui County, Yichang City, Hubei Province (**Figure 1A**). Carbonates and nodular cherts from these two sections were deposited in a shallow-water carbonate platform, which yielded abundant fossils, including bryozoans, brachiopods, fusulinids, and corals. Chert nodules in this study were collected from the Maokou Formation in the Lianziya section and the Maokou and Wujiaping formations in the Maoertang section.

3 MATERIALS AND METHODS

3.1 Sample Preparation

Fresh chert nodules were collected from the Maoertang and Lianziya sections. Thin sections were prepared for petrographic observation. Chert nodules were crushed into 200 mesh powder for geochemical analysis.

3.2 Petrographic Observation

Thin sections were observed by using a polarizing microscope (Nikon Eclipse LV100N POL). Petrographic observations were focused on the crystallization of silica and the contact between carbonates and chert nodules. Alizarin Red-S solution was applied in staining thin sections to distinguish calcite from dolomite.

3.3 Major and Trace Elemental Analyses

An aliquot of 100 mg sample powder was first leached with 10 ml of 0.5N HAc to dissolve calcareous materials. After centrifugation, the residues were washed with 5 ml of 1N HCl to completely remove the carbonate content. To completely remove Cl^- from residues, samples were washed with deionized (DI) water five times. After being dried down in an oven at 65°C, about 50 mg of sample powder was weighed and dissolved in a Teflon beaker (7 ml) by 1 ml of concentrated HNO_3 and 3 ml of concentrated HF for 24 h on a hotplate at 120°C. The solutions were dried down on a hotplate, and then the residues were dissolved by 5 ml of concentrated HNO_3 at 120°C for 24 h. After complete dissolution of samples, the solutions were dried down on a hotplate to expel excessive HNO_3. Finally, the residues were dissolved in 5 ml of 2% HNO_3 for the analysis of elemental compositions.

Major element concentrations, including ^{27}Al, ^{137}Ba, ^{40}Ca, ^{56}Fe, ^{39}K, ^{24}Mg, ^{23}Na, and ^{55}Mn, were determined by a Spectra Blue Sop inductively coupled plasma optical emission spectrometer (ICP-OES) at Peking University. Rare Earth Elements and other trace elements were analyzed by an inductively coupled plasma mass spectrometry (ICP-MS) at Chinese Academy of Geological Sciences, including ^{139}La, ^{140}Ce, ^{141}Pr, ^{144}Nd, ^{150}Sm, ^{152}Eu, ^{157}Gd, ^{159}Tb, ^{163}Dy, ^{89}Y, ^{165}Ho, ^{167}Er, ^{169}Tm, ^{173}Yb, ^{175}Lu, and ^{74}Ge contents. SiO_2 content was calculated by summing the weight of oxides of all major elements (Al_2O_3, CaO, Fe_2O_3, K_2O, MgO, and Na_2O) and minor elements to 100%. The analytical precision is better than 5% for all major elements and 10% for trace elements. Two standard materials, GSR-5 (shale) and GSR-13 (calcite), were measured to calibrate the accuracy of the determination.

4 RESULTS

4.1 Petrological Observations

The Maokou and Wujiaping formations are composed of gray limestone and bioclastic limestone/packstone in the Lianziya and Maoertang sections. Dark gray chert nodules are randomly distributed in carbonates. Chert nodules show a variety of morphologies and sizes. Most chert nodules are irregular, discontinuous, and are distributed roughly parallel to the bedding (**Figures 2A,B**). The abundance of chert nodules varies through layers (**Figure 1B**).

According to microscopic observations, the Maokou Formation in the Lianziya section is dominantly composed of limestone and bioclastic limestone/packstone (**Figures 2C,D**). Chert nodules predominantly consist of microquartz in both sections. Biological fabrics, including brachiopods, ostracods, bivalves, and sponges, could also be identified in the carbonate matrix and nodular cherts in both sections (**Figure 2**).

4.2 Geochemical Results

4.2.1 Major Elemental Compositions and Ge/Si Ratios

Major and trace elemental compositions of chert nodules in the Lianziya and Maoertang sections are presented in **Supplementary Data S1, S2**, respectively. In the Lianziya section, the SiO_2 content of the chert nodules ranges from 89.04% to 99.43%, with an average of 96.70%. Al_2O_3 and Fe_2O_3 contents range from 0.27% to 5.56% with an average of 1.77%, and 0.12%–3.11% with an average of 0.78, respectively. Germanium to silicon ratios (Ge/Si) in the Lianziya section range from 0.14 to 0.63 μmol/mol. The average Ge/Si ratio is 0.33 μmol/mol. In the Maoertang section, SiO_2 concentrations of chert nodules range from 96.42% to 99.76%, with an average of 98.80%. Al_2O_3 and Fe_2O_3 contents range from 0.10% to 2.03% with an average of 0.56% and from 0.03% to 1.39% with an average of 0.34%, respectively (**Figures 3**, **4**). Ge/Si ratios vary between 0.02 and 0.75 μmol/mol, with an average of 0.18 μmol/mol (**Figure 5**).

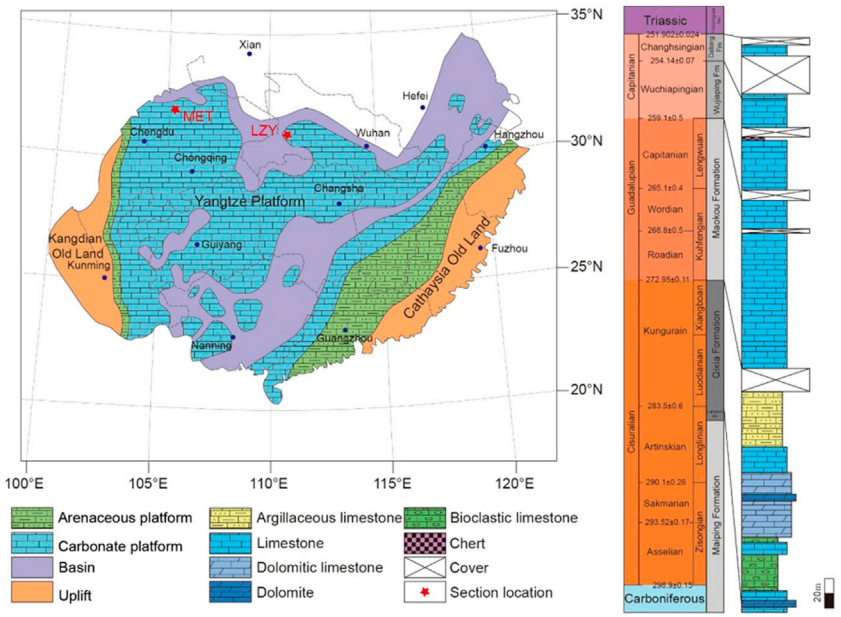

FIGURE 1 | Paleogeographic map [modified from Wang and Jin, (2000)] and the stratigraphic column in the Permian (260 Ma) of the South China Block. Sampling localities are marked by red stars. LZY: The Lianziya section, MET: The Maoertang section. The geochronology data are modified from Shen et al. (2019).

4.2.2 Rare Earth Element Compositions

In the Lianziya section, total rare earth element contents of chert samples range from 1.60 to 14.11 ppm, with an average of 5.90 ppm. The Post-Archean Australian shale (PAAS) normalized REE data display a consistent light REE (LREE) depleted pattern. Chert samples also yield low La/Yb ratios (0.24–0.84, mean = 0.55, n = 18). In addition, most samples are characterized by light negative Ce anomalies (Ce/Ce*, 0.72–0.98, mean = 0.92, n = 18), Y/Ho >1 (0.98–1.37, mean = 1.13, n = 18), and medium Eu anomalies (Eu/Eu*, 0.66–2.16, mean = 1.30, n = 18).

In the Maoertang section, the total REE contents vary within a relatively wider range, from 0.34 to 15.49 ppm, with an average of 4.21 ppm. The La/Yb ratios (0.57–2.23, mean = 1.22, n = 45) are also low, similar to those in the Lianziya section. Chert nodules in the Maoertang section also present negative Ce anomalies (0.62–1.38, mean = 0.82, n = 45). Y/Ho ratios are mostly higher than 1, ranging from 0.74 to 2.25, with an average of 1.12 (n = 45). Eu anomalies vary between 1.05 and 9.57 (mean = 2.43, n = 45), relatively higher than those of the Lianziya section (**Figure 6**), (**Supplementary Data S2**).

5 DISCUSSION

5.1 Ge/Si Ratios of Cherts in the Maokou and Wujiaping Formations

Before interpreting Ge/Si ratios of chert nodules in the Maokou and Wujiaping formations, influences from terrigenous clays and other potential contaminations should be addressed. In this study, in order to completely remove carbonate content, bulk samples were first leached by 10 ml of 0.5N HAc and 5 ml of 1N HCl. Apart from carbonaceous components, Ge can be chelated with organic matter in seawater with high DOC concentrations (Pokrovski and Schott, 1998; Pokrovski et al., 2000). Meanwhile, clay minerals can further adsorb organic matter, and thus, clay minerals typically have high Ge/Si ratios. Besides, the Ge/Si ratio of iron oxides can also reach up to 189.4 μmol/mol (Bernstein, 1985; Escoube et al., 2015). As a result, mixing with clay minerals and iron oxides would elevate Ge concentrations and Ge/Si ratios in samples.

In the Lianziya section, chert nodules are dominantly composed of SiO_2, ranging from 89.04% to 99.43% with an average of 96.70% (**Supplementary Data S1**, **Figure 4**). Al_2O_3 and Fe_2O_3 contents are relatively negligible, varying from 0.27% to 5.56% with an average of 1.77% and from 0.12% to 3.11% with an average of 0.78%, respectively (**Supplementary Data S1**) (**Figure 4**). Ge/Si ratios are low and show no significant variations, from 0.14 to 0.63 μmol/mol (mean = 0.33 μmol/mol). Besides, Ge/Si ratios are not associated with Al_2O_3 and Fe_2O_3 (**Figure 5**). Thus, Ge/Si ratios of cherts in the Lianziya section are predominantly controlled by silica content. Low Ge/Si ratios are close to those of seawater and are lower than those of hydrothermal fluids, suggesting the Si of cherts in the Lianziya section was dominantly sourced from seawater.

In the Maoertang section, SiO_2 content in cherts is higher, reaching an average level of 98.80% (**Supplementary Data S1**; **Figure 4**). Similar to the Lianziya section, the Al_2O_3 and Fe_2O_3 contents of chert nodules in the Maoertang section range from 0.10% to 2.03%, with an average of 0.56%, and from 0.03% to 1.39%, with an average of 0.34%, respectively (**Supplementary Data S1**; **Figure 4**). There is no positive correlation between Ge/Si

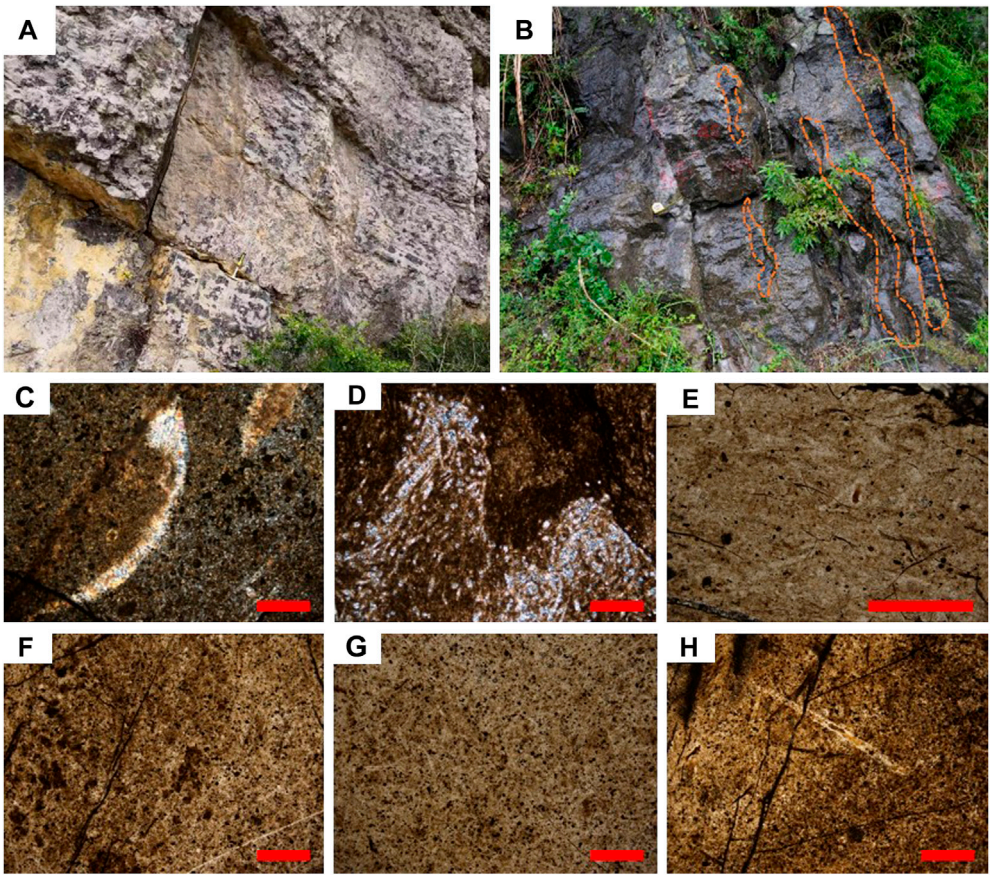

FIGURE 2 | Field photographs and photomicrographs of the Permian chert nodules. **(A)** Field photograph of the Lianziya section; **(B)** Field photograph of the Maoertang section; **(C–H)** Photomicrographs of chert nodules. Scale bars are 500 μm in **Figures 2C–H**.

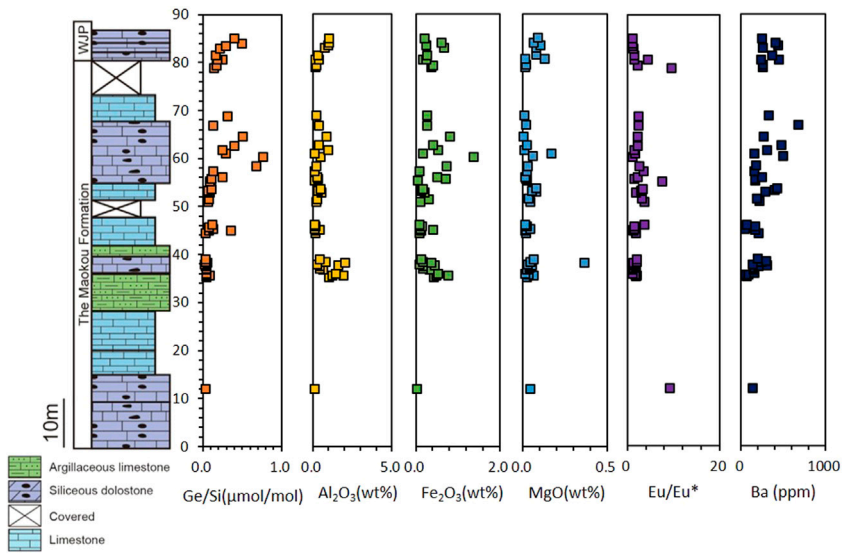

FIGURE 3 | Integrated chemostratigraphy of the Maokou and Wujiaping formations in the Maoertang section.

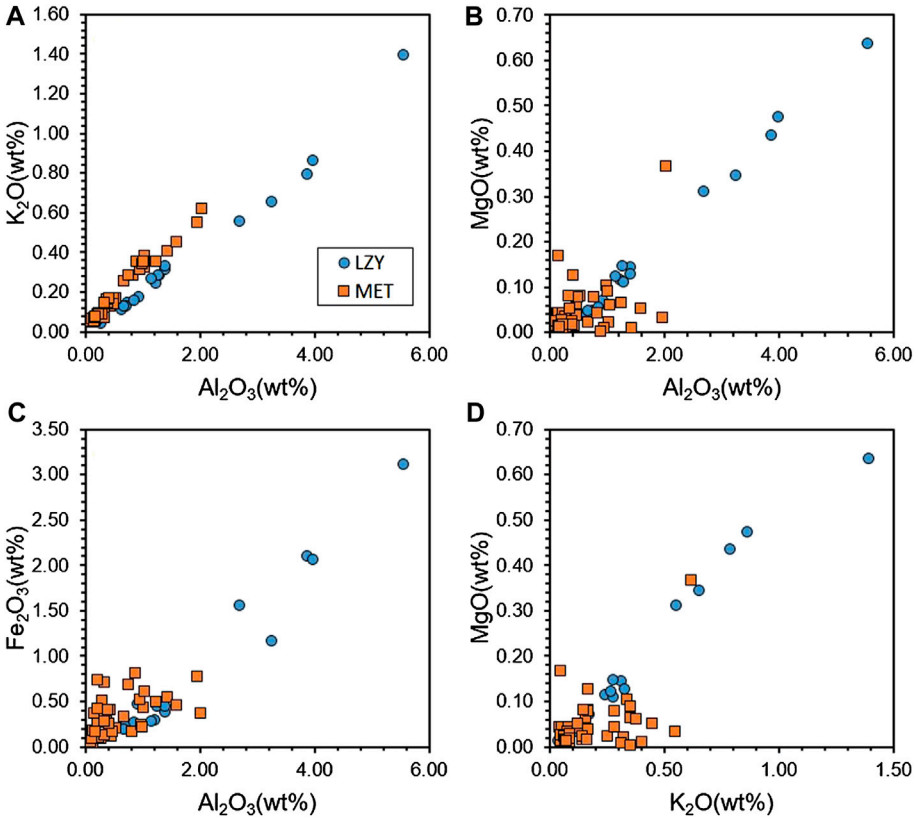

FIGURE 4 | Cross plots showing the correlations between major element contents (measured as oxides in wt%). **(A)** Al_2O_3 vs. K_2O; **(B)** Al_2O_3 vs. MgO; **(C)** Al_2O_3 vs. Fe_2O_3; and **(D)** K_2O vs. MgO.

and Al_2O_3 or Ge/Si and Fe_2O_3 (**Figure 5**) either. Therefore, the Ge/Si ratios of cherts in the Maoertang section are dominated by silica components rather than clay minerals or iron oxides.

The Ge/Si ratios in both sections suggested that Si in chert nodules predominantly originated from seawater. In the Lianziya section, Ge/Si ratios range from 0.14 to 0.63 μmol/mol, with an average of 0.33 μmol/mol. Similarly, Ge/Si ratios of the Maoertang samples are distributed between 0.02 and 0.75 μmol/mol (mean = 0.18 μmol/mol). The Ge/Si ratios of the cherts from both sections are close to the modern seawater value of 0.72 μmol/mol (King et al., 2000), which is significantly lower than that of hydrothermal fluids (5–16 μmol/mol, Escoube et al. (2015)). Thus, the Ge/Si ratios of the PCE cherts in the SCB suggest that seawater was the dominant source of Si.

5.2 REE Features of Cherts in the Maokou and Wujiaping Formations

Chert samples in the Maokou and Wujiaping formations in this study are a mix of three components: silica content, clay minerals, and iron oxides. REE patterns will be affected by the ratio of each component. Detrital clay minerals contain high total REE (TREE) concentrations that show flat REE patterns, whereas the authigenic clay minerals come from seawater, recording a seawater pattern of depleted-LREE, high Y/Ho and a negative Ce anomaly (German et al., 1991). Iron-minerals show an MREE-enrichment pattern. Neither clay minerals nor iron-minerals have Eu or Ce anomalies. The hydrothermal fluid and seawater signals will not be affected by these two components. However, the mixing of clays and iron-minerals will elevate total REE concentrations, which may dilute Eu and Ce anomalies.

In the Lianziya section, both TREE vs. Al_2O_3 and TREE vs. Fe_2O_3 show positive linear correlations (R^2 = 0.73 and 0.79, respectively), indicating that clay and iron-minerals elevate TREE concentrations (**Figure 6**). Eu/Eu* and Ce/Ce* are diluted by high Al_2O_3 and Fe_2O_3 concentrations (**Figure 6**). There is no correlation between La/Yb and Al_2O_3, Y/Ho and Al_2O_3, La/Yb and Fe_2O_3, or Y/Ho and Fe_2O_3 (**Figure 6**). All samples show LREE-depletion patterns, negative Ce anomalies (0.72–0.98, with an average of 0.92) and their La/Yb ratios are all less than 1. And 14 out of 18 samples demonstrate positive Eu anomalies (0.66–2.16, mean = 1.30, n=18).

In the Maoertang section, REE data show a similar pattern to that of the Lianziya section. TREE and Al_2O_3 show a positive linear relationship (R^2 = 0.56, **Figure 6**), while the positive correlation between TREE and Fe_2O_3 is not obvious (**Figure 6**). Eu/Eu* and Ce/Ce* are also eliminated in samples with higher Al_2O_3 and Fe_2O_3 concentrations (**Figure 6**). There is no correlation between La/Yb and Al_2O_3, Y/Ho and Al_2O_3, La/Yb and Fe_2O_3, and Y/Ho and Fe_2O_3 as well. Overall, 11 out of 45

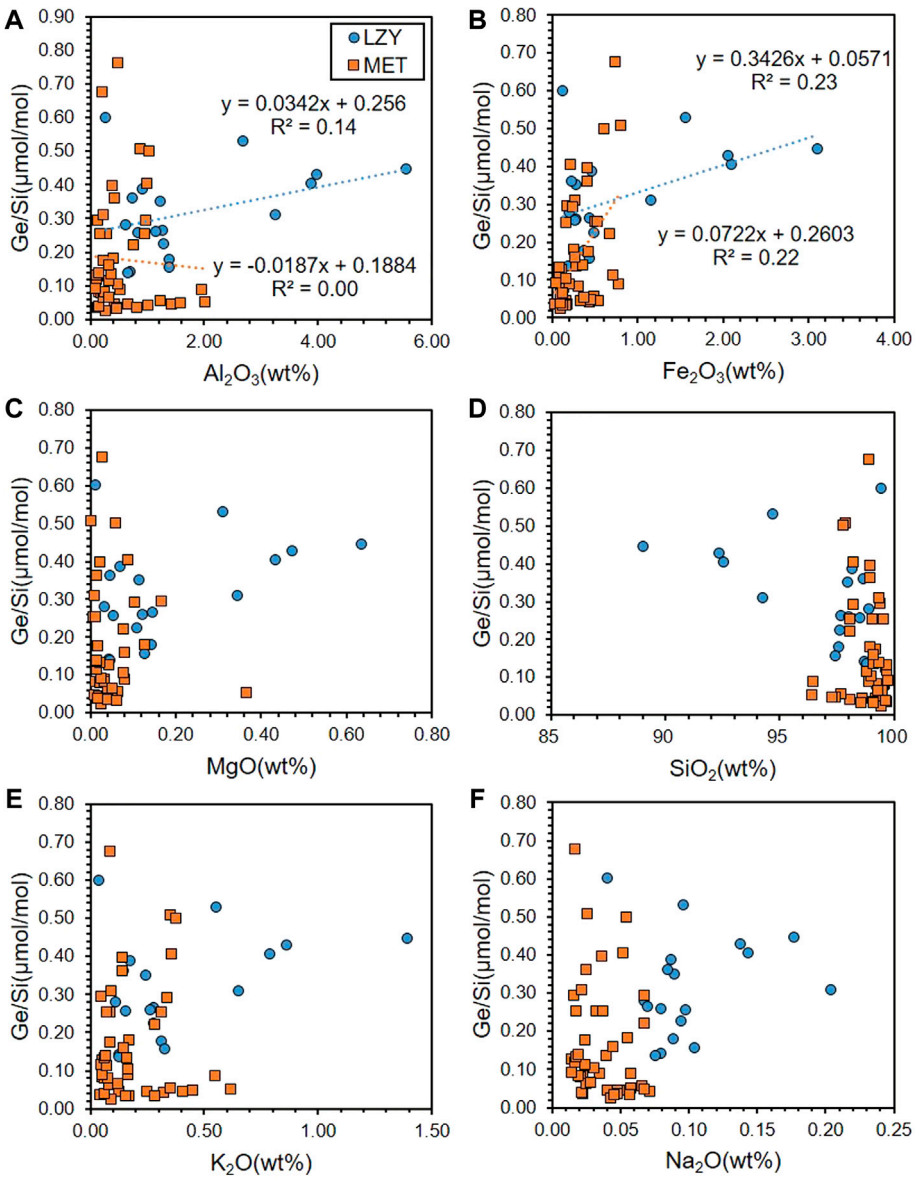

FIGURE 5 | Cross plots showing the correlations between Ge/Si (μmol/mol) and major element contents (measured as oxides in wt%). **(A)** Al_2O_3 vs. Ge/Si; **(B)** Fe_2O_3 vs. Ge/Si; **(C)** MgO vs. Ge/Si; **(D)**. SiO_2 vs. Ge/Si; **(E)** K_2O vs. Ge/Si; and **(F)** Na_2O vs. Ge/Si.

samples show LREE-depletion patterns and negative Ce anomalies (0.62–1.38, with an average of 0.82). All samples show positive Eu anomalies (1.05–9.57, mean = 2.43, n = 45). It is worth mentioning that the measurement of Sm, Eu, and Gd could also be affected by barium concentrations in ICP-MS; however, Eu/Eu* and Ba do not show positive correlations (**Figure 7F**), ruling out this possibility.

In the Lianziya and Maoertang sections, the LREE-depletion patterns, high Y/Ho ratios, and negative Ce anomalies suggest that the seawater might be the predominant Si source of chert nodules (**Figure 8**). Meanwhile, samples also show positive Eu anomalies, which is a typical hydrothermal fluids signal in chert. To resolve the conflict, we use a binary mixing model to quantify the contribution of hydrothermal fluid and seawater with regard to the Si source of chert nodules in the Maokou and Wujiaping formations from SCB.

5.3 Ge/Si-Eu/Eu * Systematics of Cherts in the Maokou and Wujiaping Formations

5.3.1 Description of Ge/Si-Eu/Eu * Model

The binary mixing model is based on two parameters, Ge/Si and Eu/Eu*, and regards seawater and hydrothermal fluids as two endmembers (Cui et al., 2019). In this model, Ge/Si and Eu/Eu* can be calculated by mass-balance equations as follows:

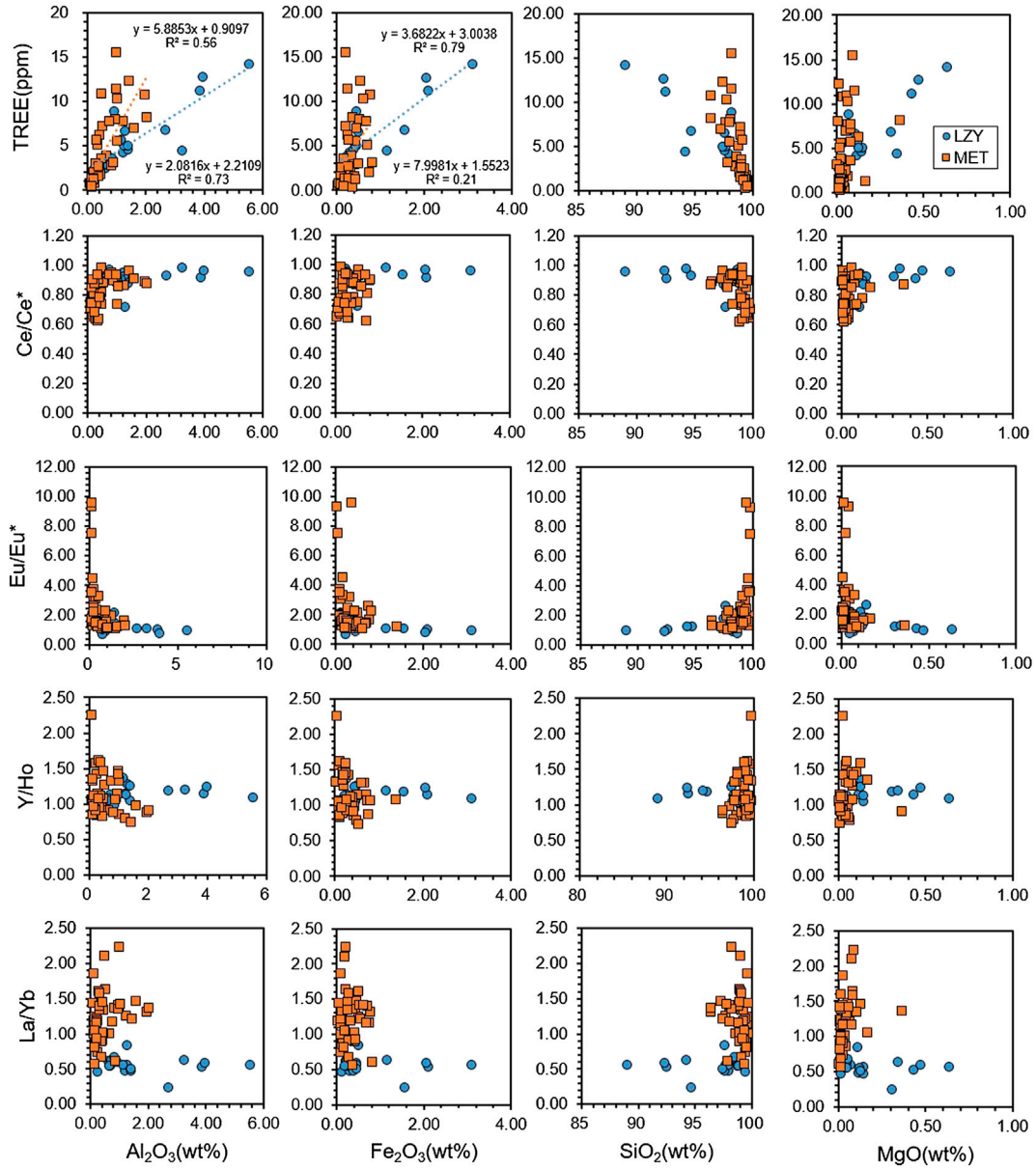

FIGURE 6 | Cross plots showing the correlations between major element contents (measured as oxides in wt%) and TREE (ppm), Ce/Ce*, Eu/Eu*, Y/Ho, and La/Yb.

$$\frac{Ge}{Si} = \frac{f \times m_{HF} \times \left(\frac{Ge}{Si}\right)_{HF} + (1-f) \times m_{SW} \times \left(\frac{Ge}{Si}\right)_{SW}}{f \times m_{HF} + (1-f) \times m_{SW}}, \quad (1)$$

$$\frac{Eu}{Eu^*} = \frac{f \times REE_{HF} \times \left(\frac{Eu}{Eu^*}\right)_{HF} + (1-f) \times REE_{SW} \times \left(\frac{Eu}{Eu^*}\right)_{SW}}{f \times REE_{HF} + (1-f) \times REE_{SW}}, \quad (2)$$

where f is the volume fraction of hydrothermal fluids and m_i represents silica concentrations (mM); $(Ge/Si)_i$ represents the Ge/Si ratio; $(Eu/Eu^*)_i$ represents the Eu anomaly; REE represents total REE concentrations (ppb); subscripts HF and SW represent the two endmembers: hydrothermal fluids and seawater, respectively.

Some parameters in hydrothermal fluids, including Eu anomaly, SiO_2 concentration and Ge/Si ratio, are strongly dependent on temperature (Douville et al., 1999). On the basis of the data collected from modern hydrothermal fluids in Lucky strike, Cruise (Douville et al., 1999), a negative correlation between Eu anomaly and temperature has been established (Cui et al., 2019), which can be expressed as:

$$\frac{Eu}{Eu^*} = -0.123 \times T + 49.604 \ (R^2 = 0.864), \quad (3)$$

where T is the temperature (in Kelvin) of hydrothermal fluids.

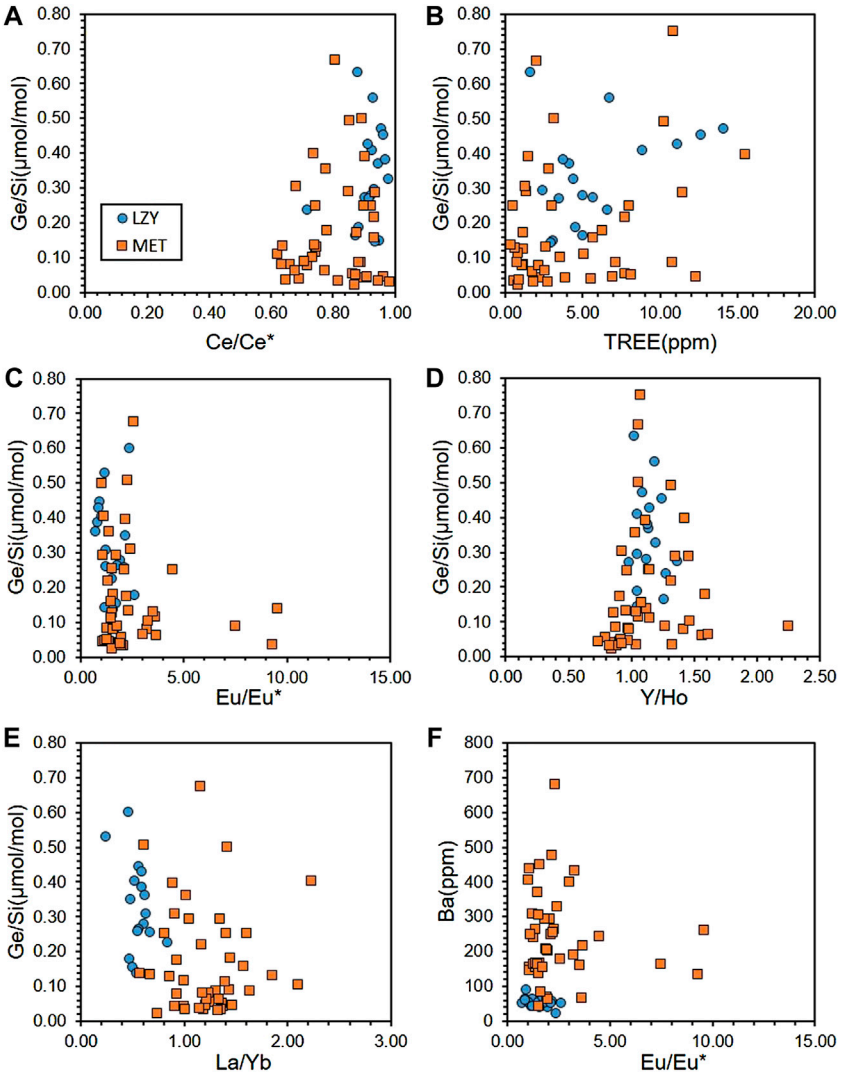

FIGURE 7 | Cross plots showing the correlations between **(A)** Ge/Si (μmol/mol) vs. TREE (ppm); **(B)** Ge/Si (μmol/mol) vs. Ce/Ce*; **(C)** Ge/Si (μmol/mol) vs. Eu/Eu*; **(D)** Ge/Si (μmol/mol) vs. Y/Ho; **(E)** Ge/Si (μmol/mol) vs. La/Yb, and **(F)** Ba (ppm) vs. Eu/Eu*.

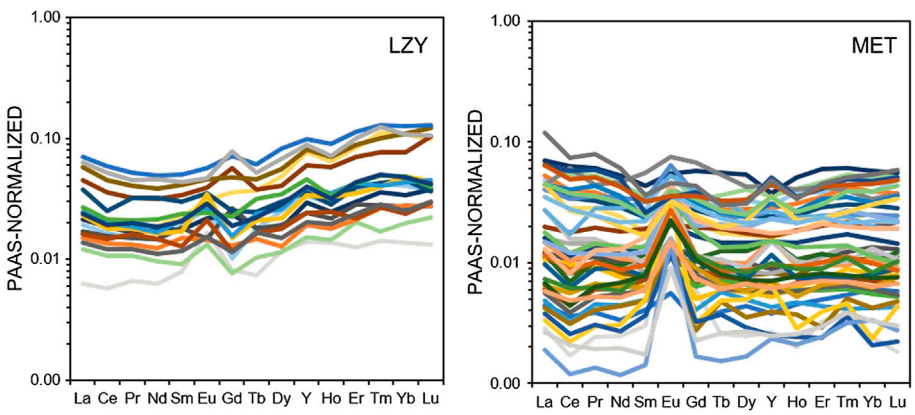

FIGURE 8 | PAAS-normalized REE patterns of the MET and LZY sections, showing the LREE depletion and the positive Eu anomaly.

TABLE 1 | Parameters of the binary-mixing model.

Parameter	Value	Unit	Range	Equation	Reference
Eu * (HF)	—	—	—	(3)	Douville et al. (1999)
SiO_2	—	mM	—	(4)	Crerar and Anderson, (1971)
Ge/Si (HT)	—	μmol/mol	—	(5)	Evans and Derry, (2002)
REE_{HF}	2	ppb	0.5–3.0	—	Douville et al. (1999)
SiO_2 (sw)	2.2	mM	0.5–2.2	—	Siever, (1992); Conley et al. (2017)
Ge/Si (sw)	0.02	μmol/mol	0.02–0.72		King et al. (2000)
REEsw	29	ppt			German and Elderfield, (1990); Douville et al. (1999)
Eu * (sw)	1.13	—			Douville et al. (1999)
Alpha	0.02	—	0.0054–0.023		Evans and Derry, (2002)
Ge/Si_0	10	μmol/mol	5–15		
T_0	400	°C	300–400		

In hydrothermal fluids, SiO_2 remains saturated with respect to quartz, and the saturation concentration is determined by temperature (Crerar and Anderson, 1971). The relationship between SiO_2 and temperature can be expressed as (Crerar and Anderson, 1971):

$$\mathrm{Log\,m} = -\frac{1107}{\mathrm{T}} - 0.0245, \tag{4}$$

where m is the saturation concentration of SiO_2 (mol) and T is the temperature of hydrothermal fluids in Kelvin. Solubility of SiO_2 usually decreases with decreasing temperature (Crerar and Anderson, 1971), so cooling of hydrothermal fluids can cause crystallization of quartz. Compared to Ge, Si preferentially enters into the lattice of quartz (Escoube et al., 2015), causing enrichment of Ge and a high Ge/Si ratio in hydrothermal fluids (Escoube et al., 2015). The development of Ge/Si ratios of hydrothermal fluids is in accordance with the Rayleigh distillation model (Evans and Derry, 2002), which can be expressed as:

$$\left(\frac{Ge}{Si}\right)_{HF} = \left(\frac{Ge}{Si}\right)_0 \times F^{\alpha-1}, \tag{5}$$

$$\mathrm{F} = [\mathrm{Si}]/[\mathrm{Si}]_0, \tag{6}$$

$$\alpha = \left((\mathrm{Ge/Si})_{\mathrm{quartz}}\right)/\left((\mathrm{Ge/Si})_{\mathrm{fluid}}\right), \tag{7}$$

where $(Ge/Si)_0$ is the Ge/Si ratio of the primary hydrothermal fluids; F is the fraction of Si in the hydrothermal system, which can be calculated by **Eq. 6**; $[Si]_0$ is the initial silica concentration, and [Si] is the remaining silica concentration; α is the fraction factor of quartz precipitation, and is defined as the instantaneous quartz Ge/Si ratio divided by the instantaneous fluid Ge/Si ratio (**Eq. 7**). α value ranges between 0.0054 and 0.023 (Evans and Derry, 2002).

5.3.2 Parameter Setting

We assume that Si concentration and REE level in seawater remain consistent and REE concentrations in hydrothermal fluids are fixed. Parameters in this model are summarized in **Table 1**.

The Ge/Si ratio of modern seawater is 0.72 μmol/mol (King et al., 2000), and it is set at 0.02 μmol/mol (minimum of sample value) in this model. SiO_2 and REE concentrations of seawater are assigned to m_{SW} = 2.2 mM and REE_{SW} = 29 ppt, respectively (Douville et al., 1999; Conley et al., 2017). Eu/Eu* of seawater is 1.13, and the seawater temperature is set at 25°C (Elderfield et al., 1988). As for hydrothermal fluid, the initial temperature T_0 and $(Ge/Si)_0$ are set as 400°C and 10 μmol/mol, respectively. Si concentration in hydrothermal fluids is 1281 ppm (Crerar and Anderson, 1971), and $(Eu/Eu^*)_{HF0}$ is set as 0.4 and change with temperature (Douville et al., 1999). Besides, REE concentration in hydrothermal fluid (REE_{HF}) is estimated at 2000 ppt (Douville et al., 1999). According to Evans and Derry (2002), parameter α distributes between 0.0054 and 0.023. In this model, α is assigned to a value of 0.02.

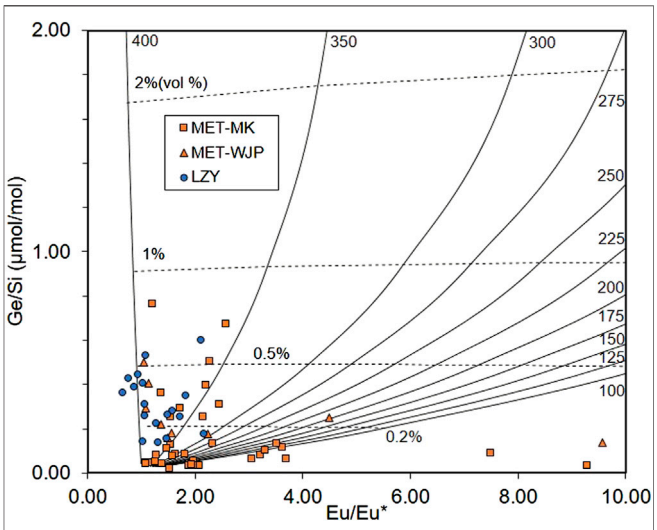

FIGURE 9 | Modeling results showing the binary mixing between hydrothermal fluid and seawater. The solid contour lines represent hydrothermal fluids of different temperatures (100–400°C), while the tick marks and the dashed lines indicate the volume fraction of hydrothermal fluid (0.2%–2%).

5.3.3 Modeling Results and Si Source of Chert Nodules in the Maokou and Wujiaping Formations

The modeling results are presented by a Eu/Eu*-Ge/Si cross-plot (**Figure 9**). The solid contour lines represent various temperatures of hydrothermal fluids, while the dashed lines

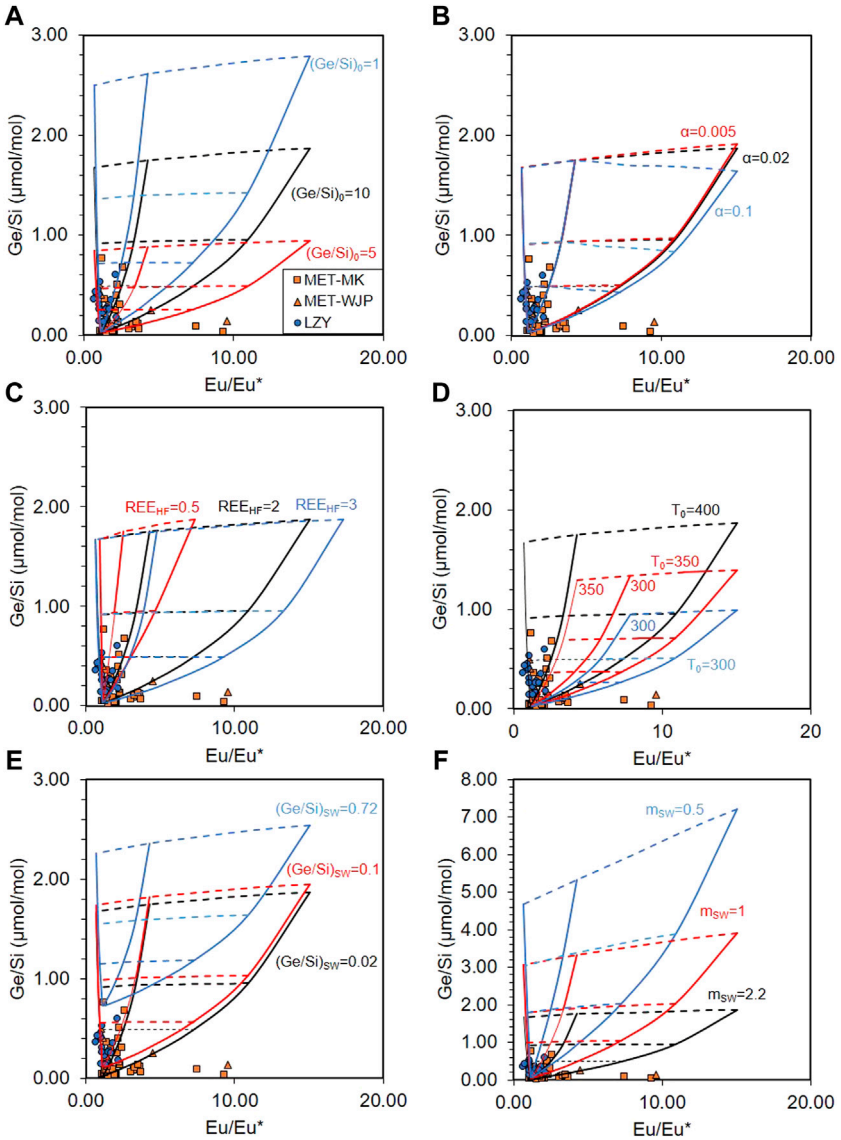

FIGURE 10 | Sensitivity tests of the binary-mixing model. The initial default parameters are $(Ge/Si)_0$ = 10 μmol/mol, α = 0.02, REE_{HF} = 2.0 ppb, T_0 = 400°C, $(Ge/Si)_{SW}$ = 0.02 μmol/mol, and m_{SW} = 2.2 mM. The sensitivity of parameters are tested by adjusting a single parameter, **(A)** $(Ge/Si)_0$; **(B)** α; **(C)** REE_{HF}; **(D)** T_0; **(E)** $(Ge/Si)_{SW}$; and **(F)** m_{SW}; while the other parameters are fixed at the default values. The contour lines represent hydrothermal fluid temperature of 400°C, 350°C, and 200°C in **(A–C)** and **(E,F)**. The dashed lines represent the volume fraction of hydrothermal fluid (2%, 1%, and 0.5%). The modeling results indicate that the estimated mixing ratios are not sensitive to the values of the aforementioned parameters.

denote the mixing volume fraction of hydrothermal fluids. Eu/Eu*-Ge/Si data of samples are plotted in **Figure 9**.

In the Lianziya section, the temperature of hydrothermal fluids ranges from 300 to 400°C, and the mixing ratio of hydrothermal influx is lower than 1 vol% (**Figure 9**). In the Maoertang section, the temperature of hydrothermal fluids in the Maokou Formation ranges from <200 to 400°C, and the mixing ratio of hydrothermal influx is lower than 1 vol% (**Figure 9**). In the Wujiaping Formation, the temperature of hydrothermal fluids ranges from 200 to 400°C, and the mixing ratio of hydrothermal influx is lower than 0.5 vol% (**Figure 9**). Thus, based on the modeling results, the temperature of hydrothermal fluids ranges from <200 to 400°C. The mixing volume fraction of hydrothermal fluids is lower than 1 vol%, equivalent to the mass fraction of 10 wt%. This indicates that the Si of cherts in the PCE was dominantly sourced from seawater, as evidenced by Ge/Si ratios and REE patterns. It is interesting to see that although the contribution fraction of hydrothermal fluids is extremely low (lower than 1 vol%), it still results in positive Eu anomalies.

5.3.4 Sensitivity Test

The modeling results could be influenced by parameter settings. To verify the reliability of the modeling results, we ran sensitivity tests for

different parameters according to their ranges (**Table 1**). The parameters that we tested include the original Ge/Si ratio of hydrothermal fluids (Ge/Si_0), the fractionation during hydrothermal quartz precipitation (α), the REE concentration of hydrothermal fluids (REE_{HF}), the initial temperature of hydrothermal fluid (T_0), the Ge/Si ratio of seawater (Ge/Si_{SW}), and the SiO_2 concentration of seawater (m_{SW}). Results of sensitivity tests indicate that the estimated mixing of 1 vol% of hydrothermal fluids is not significantly influenced by the tested parameters (**Figure 10**).

5.4 Implications of Positive Eu Anomaly in Determining Hydrothermal Source of Siliceous Precipitation

The Eu anomaly has long been regarded as a direct proxy for the implicated hydrothermal fluid source of Si in the chert formation. However, in this study, although the chert samples in PCE show significant Eu/Eu*[The Lianziya section: 0.66 to 2.16 (mean = 1.30, *n*=18); the Maoertang section: 1.05 to 9.57 (mean = 2.43, *n* = 45)], their contribution fraction is rather low (1 vol%). In addition, low Ge/Si ratios and LREE-depleted REE patterns also strongly argue for the contemporaneous seawater origin of the Permian chert nodules.

In fact, Eu/Eu* in hydrothermal fluids and in seawater have a great variation of 14.17 to 1.13, which means that a small fraction of hydrothermal fluids could highly influence the Eu/Eu* of bulk samples. Enriched elements in hydrothermal fluids could have a very high concentration that is one order of magnitude higher than that in seawater, making these elements ineffective in tracing Si source of chert nodules. Therefore, a positive Eu anomaly does not necessarily indicate hydrothermal-sourced Si in cherts. In order to accurately determine the Si source of cherts, the Ge/Si ratio and REE pattern should also be carefully considered.

6 CONCLUSION

We measured Ge/Si ratios and REE compositions of chert nodules of the Maokou and Wujiaping formations from two sections in South China. Samples show low Ge/Si ratios (0.02–0.75 μmol/mol), LREE-depleted patterns and positive Eu anomalies, suggesting seemingly conflicting contemporaneous seawater and hydrothermal fluid origins of the PCE chert nodules. It is demonstrated, however, by a binary-mixing model with seawater and hydrothermal fluids as two endmembers, that hydrothermal fluids only account for 1 vol % of the Si source in the chert nodules, and seawater is the major source. This study suggests that a small amount of hydrothermal fluid can lead to a high Eu anomaly, and therefore, the Eu anomaly may not always be an effective proxy in determining the silicon source of cherts; instead, Ge/Si ratio and REE patterns should also be considered.

DATA AVAILABILITY STATEMENT

The original contributions presented in the study are included in the article/**Supplementary Material**; further inquiries can be directed to the corresponding authors.

AUTHOR CONTRIBUTIONS

Conceptualization: LD; Resources: LD, YC, CQL, MN, CX, and PX; Visualization: CQL, YC, and MN; Formal analysis: CQL and CL; Writing—original draft: LD, CQL, YC, CX, and MN; Writing—review and editing: LD, YC, CQL, and MN.

FUNDING

This work is supported by the Natural Science Foundation of China 42090021.

ACKNOWLEDGMENTS

We thank the editor and two reviewers' constructive comments and suggestions which improved the manuscript.

SUPPLEMENTARY MATERIAL

The Supplementary Material for this article can be found online at: https://www.frontiersin.org/articles/10.3389/feart.2022.932263/full#supplementary-material

REFERENCES

Alibert, C., and Kinsley, L. (2016). Ge/Si in Hamersley BIF as Tracer of Hydrothermal Si and Ge Inputs to the Paleoproterozoic Ocean. *Geochimica Cosmochimica Acta* 184, 329–343. doi:10.1016/j.gca.2016.03.027

Alibo, D. S., and Nozaki, Y. (1999). Rare Earth Elements in Seawater: Particle Association, Shale-Normalization, and Ce Oxidation. *Geochimica Cosmochimica Acta* 63 (3–4), 363–372. doi:10.1016/s0016-7037(98)00279-8

Bareille, G., Labracherie, M., Mortlock, R. A., Maier-Reimer, E., and Froelich, P. N. (1998). A Test of (Ge/Si)opal as a Paleorecorder of (Ge/Si)seawater. *Geol* 26 (2), 179–182. doi:10.1130/0091-7613(1998)026<0179:atogso>2.3.co;2

Baronas, J. J., Hammond, D. E., Mcmanus, J., Wheat, C. G., and Siebert, C. (2017). A Global Ge Isotope Budget. *Geochimica Cosmochimica Acta* 203, 265–283. doi:10.1016/j.gca.2017.01.008

Bau, M. (1991). Rare-earth Element Mobility during Hydrothermal and Metamorphic Fluid Rock Interaction and the Significance of the Oxidation-State of Europium. *Chem. Geol.* 93 (3-4), 219–230. doi:10.1016/0009-2541(91)90115-8

Beauchamp, B., and Baud, A. (2002). Growth and Demise of Permian Biogenic Chert along Northwest Pangea: Evidence for End-Permian Collapse of Thermohaline Circulation. *Palaeogeogr. Palaeoclimatol. Palaeoecol.* 184 (1-2), 37–63. doi:10.1016/s0031-0182(02)00245-6

Bernstein, L. R. (1985). Germanium Geochemistry and Mineralogy. *Geochimica Cosmochimica Acta* 49 (11), 2409–2422. doi:10.1016/0016-7037(85)90241-8

Bernstein, L. R., and Waychunas, G. A. (1987). Germanium Crystal Chemistry in Hematite and Goethite from the Apex Mine, Utah, and Some New Data on Germanium in Aqueous Solution and in Stottite. *Geochimica Cosmochimica Acta* 51 (3), 623–630. doi:10.1016/0016-7037(87)90074-3

Conley, D. J., Frings, P. J., Fontorbe, G., Clymans, W., Stadmark, J., Hendry, K. R., et al. (2017). Biosilicification drives a decline of dissolved si in the oceans through geologic time. *Front. Mar. Sci.* 4 (397). doi:10.3389/fmars.2017.00397

Crerar, D. A., and Anderson, G. M. (1971). Solubility and Solvation Reactions of Quartz in Dilute Hydrothermal Solutions. *Chem. Geol.* 8 (2), 107–122. doi:10.1016/0009-2541(71)90052-0

Cui, Y., Lang, X., Li, F., Huang, K., Ma, H., Li, C., et al. (2019). Germanium/silica Ratio and Rare Earth Element Composition of Silica-Filling in Sheet Cracks of the Doushantuo Cap Carbonates, South China: Constraining Hydrothermal Activity during the Marinoan Snowball Earth Glaciation. *Precambrian Res.* 332, 105407. doi:10.1016/j.precamres.2019.105407

Deng, T., Li, Y., and Hu, X. (2022). Origin of Carnian Ma'antang Cherts, Northwestern Sichuan Basin, South China: Field, Petrographic, and Geochemical Perspectives. *J. Asian earth Sci.* 228, 105143. doi:10.1016/j.jseaes.2022.105143

Dong, L., Shen, B., Lee, C.-T. A., Shu, X.-j., Peng, Y., Sun, Y., et al. (2015). Germanium/silicon of the Ediacaran-Cambrian Laobao Cherts: Implications for the Bedded Chert Formation and Paleoenvironment Interpretations. *Geochem. Geophys. Geosyst.* 16 (3), 751–763. doi:10.1002/2014gc005595

Dong, Y., Xu, S., Wen, L., Chen, H., Fu, S., Zhong, Y., et al. (2020). Tectonic Control of Guadalupian-Lopingian Cherts in Northwestern Sichuan Basin, South China. *Palaeogeogr. Palaeoclimatol. Palaeoecol.* 557, 109915. doi:10.1016/j.palaeo.2020.109915

Douville, E., Bienvenu, P., Charlou, J. L., Donval, J. P., Fouquet, Y., Appriou, P., et al. (1999). Yttrium and Rare Earth Elements in Fluids from Various Deep-Sea Hydrothermal Systems. *Geochimica cosmochimica acta* 63 (5), 627–643. doi:10.1016/S0016-7037(99)00024-1

Elderfield, H., Charnock, H., Lovelock, J. E., Liss, P. S., and Whitfield, M. (1988). The Oceanic Chemistry of the Rare-Earth Elements. *Phil. Trans. R. Soc. Lond. A* 325 (1583), 105–126. doi:10.1098/rsta.1988.0046

Escoube, R., Rouxel, O. J., Edwards, K., Glazer, B., and Donard, O. F. X. (2015). Coupled Ge/Si and Ge Isotope Ratios as Geochemical Tracers of Seafloor Hydrothermal Systems: Case Studies at Loihi Seamount and East Pacific Rise 9°50′N. *Geochimica Cosmochimica Acta* 167, 93–112. doi:10.1016/j.gca.2015.06.025

Evans, M. J., and Derry, L. A. (2002). Quartz Control of High Germanium/silicon Ratios in Geothermal Waters. *Geol* 30 (11), 1019–1022. doi:10.1130/0091-7613(2002)030<1019:qcohgs>2.0.co;2

Froelich, P. N., Blanc, V., Mortlock, R. A., Chillrud, S. N., Dunstan, W., Udomkit, A., et al. (1992). River Fluxes of Dissolved Silica to the Ocean Were Higher during Glacials: Ge/Si in Diatoms, Rivers, and Oceans. *Paleoceanography* 7 (6), 739–767. doi:10.1029/92pa02090

Gao, P., He, Z., Lash, G. G., Li, S., Xiao, X., Han, Y., et al. (2020). Mixed Seawater and Hydrothermal Sources of Nodular Chert in Middle Permian Limestone on the Eastern Paleo-Tethys Margin (South China). *Palaeogeogr. Palaeoclimatol. Palaeoecol.* 551, 109740. doi:10.1016/j.palaeo.2020.109740

Gates, L. M., James, N. P., and Beauchamp, B. (2004). A Glass Ramp: Shallow-Water Permian Spiculitic Chert Sedimentation, Sverdrup Basin, Arctic Canada. *Sediment. Geol.* 168 (1-2), 125–147. doi:10.1016/j.sedgeo.2004.03.008

German, C. R., and Elderfield, H. (1990). Rare Earth Elements in the NW Indian Ocean. *Geochimica Cosmochimica Acta* 54 (7), 1929–1940. doi:10.1016/0016-7037(90)90262-j

German, C. R., Holliday, B. P., and Elderfield, H. (1991). Redox Cycling of Rare Earth Elements in the Suboxic Zone of the Black Sea. *Geochimica Cosmochimica Acta* 55 (12), 3553–3558. doi:10.1016/0016-7037(91)90055-a

Guan, Z., Deng, S., Liu, P., Jin, Y., and Cao, X. (2020). Germanium/silica Ratio and Trace Element Composition of Early Cambrian Siliceous Rocks in Keping: Implications for the Siliceous Rocks' Formation and Paleoenvironment Interpretations. *Acta Geochim.* 39 (6), 797–810. doi:10.1007/s11631-020-00436-0

Kato, Y., and Nakamura, K. (2003). Origin and Global Tectonic Significance of Early Archean Cherts from the Marble Bar Greenstone Belt, Pilbara Craton, Western Australia. *Precambrian Res.* 125 (3-4), 191–243. doi:10.1016/S0301-9268(03)00043-3

King, S. L., Froelich, P. N., and Jahnke, R. A. (2000). Early Diagenesis of Germanium in Sediments of the Antarctic South Atlantic: in Search of the Missing Ge Sink. *Geochimica Cosmochimica Acta* 64 (8), 1375–1390. doi:10.1016/S0016-7037(99)00406-8

Liu, Z., Yuan, B., Huang, X., Dai, X., Lin, W., Mu, L., et al. (2020). Division and Correlation of Permian Formation at Maoertang Section in Northwest Sichuan, China. *Chengdu gong xue xue bao. Zi ke xue ban* 47 (3), 257–273. doi:10.3969/j.issn.1671-9727.2020.03.01

Maliva, R. G., Knoll, A. H., and Siever, R. (1989). Secular Change in Chert Distribution: A Reflection of Evolving Biological Participation in the Silica Cycle. *Palaios* 4 (6), 519–532. doi:10.2307/3514743

Maliva, R. G., Knoll, A. H., and Simonson, B. M. (2005). Secular Change in the Precambrian Silica Cycle: Insights from Chert Petrology. *Geol. Soc. Am. Bull.* 117 (7), 835–845. doi:10.1130/b25555.1

Mills, R. A., and Elderfield, H. (1995). Rare Earth Element Geochemistry of Hydrothermal Deposits from the Active TAG Mound, 26°N Mid-Atlantic Ridge. *Geochimica Cosmochimica Acta* 59 (17), 3511–3524. doi:10.1016/0016-7037(95)00224-n

Mortlock, R. A., Froelich, P. N., Feely, R. A., Massoth, G. J., Butterfield, D. A., and Lupton, J. E. (1993). Silica and Germanium in Pacific Ocean Hydrothermal Vents and Plumes. *Earth Planet. Sci. Lett.* 119 (3), 365–378. doi:10.1016/0012-821x(93)90144-x

Murray, R. W., Buchholtz Ten Brink, M. R., Gerlach, D. C., Russ, G. P., and Jones, D. L. (1991). Rare Earth, Major, and Trace Elements in Chert from the Franciscan Complex and Monterey Group, California: Assessing REE Sources to Fine-Grained Marine Sediments. *Geochimica Cosmochimica Acta* 55 (7), 1875–1895. doi:10.1016/0016-7037(91)90030-9

Murray, R. W. (1994). Chemical-criteria to Identify the Depositional Environment of Chert - General-Principles and Applications. *Sediment. Geol.* 90 (3-4), 213–232. doi:10.1016/0037-0738(94)90039-6

Pokrovski, G. S., Martin, F., Hazemann, J. L., and Schott, J. (2000). An X-Ray Absorption Fine Structure Spectroscopy Study of Germanium-Organic Ligand Complexes in Aqueous Solution. *Chem. Geol.* 163 (1), 151–165. doi:10.1016/s0009-2541(99)00102-3

Pokrovski, G. S., and Schott, J. (1998). Thermodynamic Properties of Aqueous Ge(IV) Hydroxide Complexes from 25 to 350°C: Implications for the Behavior of Germanium and the Ge/Si Ratio in Hydrothermal Fluids. *Geochimica Cosmochimica Acta* 62 (9), 1631–1642. doi:10.1016/s0016-7037(98)00081-7

Racki, G. (1999). Silica-secreting Biota and Mass Extinctions: Survival Patterns and Processes. *Palaeogeogr. Palaeoclimatol. Palaeoecol.* 154 (1-2), 107–132. doi:10.1016/s0031-0182(99)00089-9

Regional Geology of Sichuan Province (1991). *Sichuan Bureau of Geology and Mineral Resources*. Beijing: Geological Publishing House.

Shellnutt, J. G. (2014). The Emeishan Large Igneous Province: A Synthesis. *Geosci. Front.* 5 (3), 369–394. doi:10.1016/j.gsf.2013.07.003

Shemesh, A., Mortlock, R. A., and Froelich, P. N. (1989). Late Cenozoic Ge/Si Record of Marine Biogenic Opal: Implications for Variations of Riverine Fluxes to the Ocean. *Paleoceanography* 4 (3), 221–234. doi:10.1029/PA004i003p00221

Shen, B. H, S. S. Z., Hou, Z. S., Wu, Q., Zhang, S. C., Zhang, B., Zhang, Y. C., et al. (2021). Lithostratigraphic Subdivision and Correlation of the Permian in China. *J. Stratigr.* 45, 319–339. doi:10.19839/j.cnki.dcxzz.2021.0027

Shen, B., Lee, C. T. A., and Xiao, S. (2011). Germanium/silica Ratios in Diagenetic Chert Nodules from the Ediacaran Doushantuo Formation, South China. *Chem. Geol.* 280 (3), 323–335. doi:10.1016/j.chemgeo.2010.11.019

Shen, B., Ma, H., Ye, H., Lang, X., Pei, H., Zhou, C., et al. (2018). Hydrothermal Origin of Syndepositional Chert Bands and Nodules in the Mesoproterozoic Wumishan Formation: Implications for the Evolution of Mesoproterozoic Cratonic Basin, North China. *Precambrian Res.* 310, 213–228. doi:10.1016/j.precamres.2018.03.007

Shen, S., Zhang, H., Zhang, Y., Yuan, D., Chen, B., He, W., et al. (2019). Permian Integrative Stratigraphy and Timescale of China. *Sci. China Earth Sci.* 62 (1), 154–188. doi:10.1007/s11430-017-9228-4

Sholkovitz, E. R. (1992). Chemical Evolution of Rare Earth Elements: Fractionation between Colloidal and Solution Phases of Filtered River Water. *Earth Planet. Sci. Lett.* 114 (1), 77–84. doi:10.1016/0012-821X(92)90152-L

Sholkovitz, E. R., Landing, W. M., and Lewis, B. L. (1994). Ocean Particle Chemistry: The Fractionation of Rare Earth Elements between Suspended Particles and Seawater. *Geochimica cosmochimica acta* 58 (6), 1567–1579. doi:10.1016/0016-7037(94)90559-2

Siever, R. (1992). The Silica Cycle in the Precambrian. *Geochimica Cosmochimica Acta* 56 (8), 3265–3272. doi:10.1016/0016-7037(92)90303-Z

Soyol-Erdene, T.-O., and Huh, Y. (2013). Rare Earth Element Cycling in the Pore Waters of the Bering Sea Slope (IODP Exp. 323). *Chem. Geol.* 358, 75–89. doi:10.1016/j.chemgeo.2013.08.047

Sugitani, K. (1992). Geochemical Characteristics of Archean Cherts and Other Sedimentary Rocks in the Pilbara Block, Western Australia: Evidence for Archean Seawater Enriched in Hydrothermally-Derived Iron and Silica. *Precambrian Res.* 57 (1-2), 21–47. doi:10.1016/0301-9268(92)90093-4

Tatzel, M., von Blanckenburg, F., Oelze, M., Bouchez, J., and Hippler, D. (2017). Late Neoproterozoic Seawater Oxygenation by Siliceous Sponges. *Nat. Commun.* 8 (1), 1–10. doi:10.1038/s41467-017-00586-5

Tribovillard, N., Bout-Roumazeilles, V., Riboulleau, A., Baudin, F., Danelian, T., and Riquier, L. (2011). Transfer of Germanium to Marine Sediments: Insights from its Accumulation in Radiolarites and Authigenic Capture under Reducing Conditions. Some Examples through Geological Ages. *Chem. Geol.* 282 (3-4), 120–130. doi:10.1016/j.chemgeo.2011.01.015

Tribovillard, N. (2013). The Ge/Si Ratio as a Tool to Recognize Biogenic Silica in Chert. *Comptes Rendus Geosci.* 345 (3), 160–165. doi:10.1016/j.crte.2013.02.005

Wang, Y., and Jin, Y. (2000). Permian Palaeogeographic Evolution of the Jiangnan Basin, South China. *Palaeogeogr. Palaeoclimatol. Palaeoecol.* 160 (1-2), 35–44. doi:10.1016/s0031-0182(00)00043-2

Yao, X., Li, S., Zhou, Y., and Hinnov, L. A. (2021). Hydrothermal Origin of Early Permian Chert Nodules in the Central North China Craton Linked to Northern Margin Cratonic Activation. *Acta Geol. Sin. - Engl. Ed.* 95 (2), 541–557. doi:10.1111/1755-6724.14649

Yao, X., Zhou, Y., Li, S., and Li, D. (2013). Research Status and Advances in Chert and Permian Chert Event. *Adv. Earth Sci.* 28 (11), 1189.

Yu, Y., Lin, L., Deng, X., Wang, Y., Li, Y., and Guo, Y. (2020). Geochemical Features of the Middle-Upper Permian Cherts and Implications for Origin, Depositional Environment in the Sichuan Basin, SW China. *Geol. J.* 55 (2), 1493–1506. doi:10.1002/gj.3511

Zheng, H., Wu, J., Tang, H., Liu, B., Yang, X., Shi, K., et al. (2021). Origin of the Multiple-Sourced Cherts in Maokou Carbonates in Sichuan Basin, South China. *Minerals* 11 (11), 1269. doi:10.3390/min11111269

Conflict of Interest: The authors declare that the research was conducted in the absence of any commercial or financial relationships that could be construed as a potential conflict of interest.